RSC Advances

ROYAL SOCIETY OF CHEMISTRY

www.rsc.org/advances

ARTICLE TYPE www. rsc.org/xxxxxx | XXXXXXXX

Online determination of anisotropy during cellulose nanofibril assembly in a flow focusing device

Karl M. O. Håkansson,[*a,b]

Received Xth XXXXXXXXXX 20XX, Accepted Xth XXXXXXXXX 20XX
First published on the web Xth XXXXXXXXXX 200X
DOI: 10.1039/b000000x

In order to utilize the high strength (ultimate tensile strength = 3 GPa) [Saito *et al.* 2012 *Biomacromolecules* **14**, 248] and stiffness (Young's Modulus = 130 GPa) [Sakurada *et al.* 1962 *J. Polym. Sci.* **57**, 651] of cellulose nanofibrils in a macroscopic material or composite, the structure of the elongated fibrils in the material must be controlled. Here, cellulose nanofibrils in a dispersed state are partly aligned in a flow focusing device, whereafter the anisotropic nano-structure is locked by a dispersion-gel transition. The alignment process has been studied by Håkansson *et al.* 2014 [*Nat. Commun.* **5**, 4018], however, the location of the phase transition as well as at which alignment (anisotropy) the fibrils were locked was not investigated. In this study, the degree of alignment is determined with small angle X-ray scattering experiments and the location of the phase change is measured with polarized light experiments. Furthermore, the anisotropy of the hydrogel thread is determined and the thread is seen to still be anisotropic after six months in a water bath.

1 Introduction

Nano-scale building blocks have become more and more important in today's material manufacturing. In order to utilize the full potential of the the nano-scale building blocks in for example composites, the structure on the nano-scale must also be considered[1]. Hence, processes are needed in order to create well defined nano-structures as well as non-expensive online characterization methods. In this work, the alignment of dispersed cellulose nanofibrils (CNF) in an extensional flow is studied in a flow focusing channel. After the alignment, an ion-diffusion based phase transition is induced and a hydrogel thread (with an anisotropic orientation distribution of the fibrils) is formed, similar to those obtained by Fall *et al.*, Hamedi *et al.*, Håkansson *et al.*. However, in the previous studies by Hamedi *et al.*, Håkansson *et al.*, the fibrils were only roughly aligned in the direction of the thread. Moreover, the degree of alignment at the gelation position in the channel was not measured. A similar approach to produce silk from silk protein was reported by Kinahan *et al.*, where the properties of the man-made silk were rather far from those of native silk and it was unclear if the extensional flow in the channel aligned the proteins at all. Here, synchrotron Small Angle X-ray Scattering (SAXS) is used to characterize the fibril alignment in the channel without the phase transition. Thereafter, the non-expensive polarized optical microscopy (POM) is utilized to determine the location of the phase transition and the anisotropy (of the nano-structure) within the hydrogel. With this method, the degree of alignment for different configurations can be measured without having the expensive synchrotron facility at hand more than once. When well defined hydrogel threads with different and known anisotropy are created, the material properties can be characterized and later designed for a specific application. The anisotropic cellulose nanofibril hydrogels could be used, for example, as templates[6,7] or be dried to create high performance filaments[3,4].

The nano-scale building block of a wood fibre is the CNF, which in turn consist of a bundle of cellulose polymer chains. The mechanical properties of the wood fibre are highly dependent on the orientation/alignment of the nanofibrils in the fibre[8–11]. When all fibrils are perfectly aligned in the direction of the fibre, the fibre is as strong as glass fibre[12] and as stiff as Kevlar[13]. So far, only nature itself has been able to achieve this highly aligned structure. Even though cellulose has always been of large interest due to its abundance, cellulose nanofibrils (CNF) and materials thereof have recently been given a lot of attention[2,7,14–17], partly due to the a new process which significantly decreases the energy consumption during liberation of fibrils from fibres[18].

Fall *et al.* studied the dispersion-gel transition of a water based fibril dispersion and found that surface charged fibrils underwent a transition from dispersion to gel at low pH and/or high NaCl concentrations. This insight made it possible to produce aligned macro scale filaments in a flow focusing device[4], where the properties of a tree fibre was reproduced at

[a]*Wallenberg Wood Science Center, KTH Royal Institute of Technology, SE-100 44 Stockholm, Sweden. Tel: XX XXXX XXXX; E-mail: karlh@mech.kth.se*
[b]*Linné Flow Centre, Department of Mechanics, KTH Royal Institute of Technology, SE-100 44 Stockholm, Sweden. E-mail: karlh@mech.kth.se*

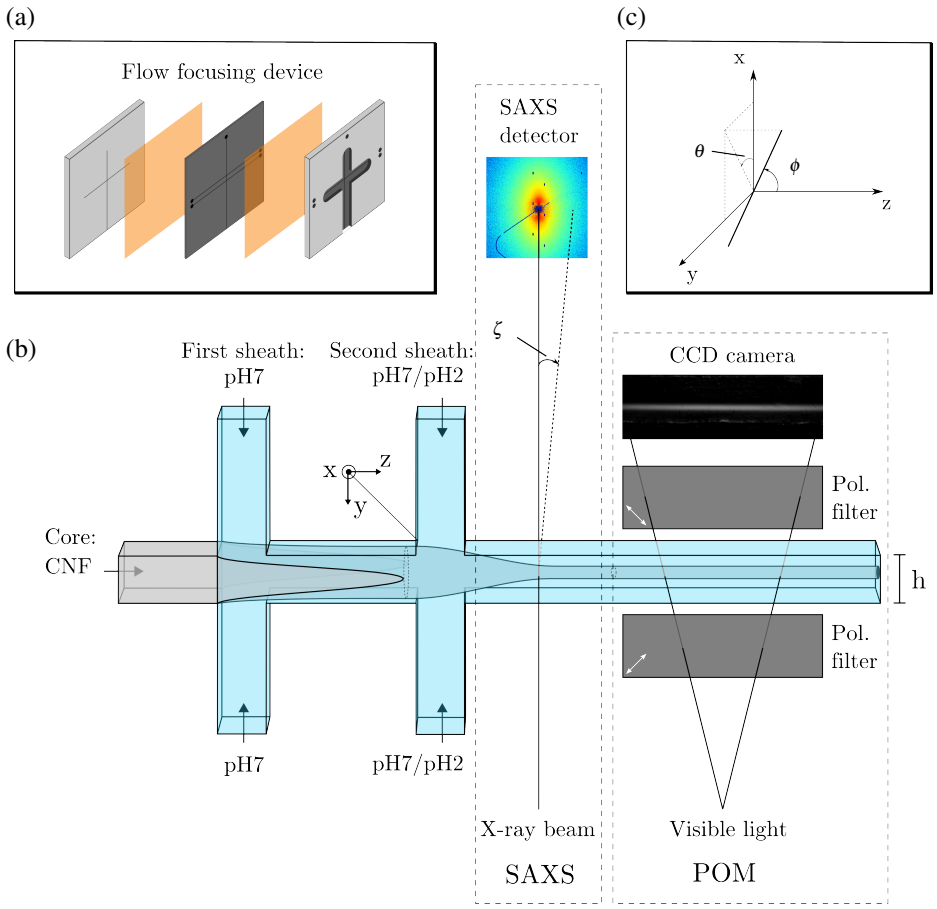

Fig. 1 A schematic of the sandwich structure of the flow focusing device is displayed in (a). A drawing of the double flow focusing channel and illustration of the two different analysis methods are shown in (b). The coordinate system for the fibrils is defined in (c).

the same fibril alignment for the first time. However, the minimum mean angle of the fibrils produced was only 35° from the filament axis, and an increase in anisotropy (decrease in mean angle) would potentially result in as stiff and strong filaments as nature can produce[8,9]. The complete process uses a dispersion of CNF which is subjected to an extensional flow inside the flow device[20,21], where fibrils were shown to align in the flow direction[4,22]. However, the problem is that when the extensional flow stops, rotary Brownian diffusion takes over and forces the aligned fibrils back towards isotropy. In order to prevent the de-alignment, Na^+-ions were allowed to diffuse into the core dispersion[23], inducing a transition to gel which was hypothesized by Håkansson *et al.* to lock the alignment. The hydrogel threads ejected from the flow device were dried and the nano-structure of the fibrils were shown to be anisotropic, *i.e.* the mean orientation of the fibrils were not random. Furthermore, the anisotropy could be controlled by small adjustments to the flow and diffusion parameters. The production of the anisotropic hydrogel is therefore crucially dependent on where the locking is achieved, since the Brownian rotary diffusion forces the fibrils back towards isotropy. Hence, in order to increase the alignment in the channel and thus also in the hydrogel, by locking the alignment at an optimal location, in situ orientation measurements are needed.

The flow focusing channel used in order to create the extensional flow consist of three inlets and one outlet, where the core flow is focused by two perpendicularly incoming sheath flows[20]. The extensional (elongational) flow is crucial for the orientation and forces elongated particles to align in the flow direction[24,25]. Several publications report on the production of filaments with different shapes[26–28], in a flow focusing device whereas others focused on the alignment and assembly[4,22,29], of elongated particles in such devices. Here, a protocol for measuring the absolute alignment and the location of the locking of the alignment online in the flow focusing channel will be presented.

Three experiments in a double flow focusing setup (depicted in Fig. 1) with and without a dispersion gel transition

Table 1 Table of experiments and cases.

Experiment number	Parameter case	Core material	First sheath	Second sheath	Gelation	Experimental setup
i	Reference	CNF	pH 7	pH 7	-	SAXS
ii	Reference	CNF	pH 7	pH 7	-	POM
iii	Process	CNF	pH 7	pH 2	x	POM

are presented, see Tab. 1. The first experiment (i) is a SAXS experiment, where the absolute orientation along the centreline is measured. Due to clogging in the channel and limited optical access in the experimental hutch, the SAXS measurement could only be performed without the gelation (pH 7 in both sheath flows). The second (ii) and third (iii) experiments are non-expensive polarized optical microscopy (POM) measurements, where the flow parameters of (ii) are the same as (i). Experiment no. (iii) represents the hydrogel manufacturing case, where the second sheath flow is a pH 2 solution which diffuses into the CNF dispersion and induces the gelation. The POM measurements, (ii) and (iii), will with the current setup only give a relative orientation measure along the channel. However, by combining the three experiments, the location of gelation as well as the orientation of the fibrils at this location, can be determined.

Finally, a hydrogel thread is produced and stored in water (pH 7) at room temperature for six months. After that time the thread still shows a birefringence indicating that the anisotropy is still present.

2 Methods

2.1 Materials

Cellulose nanofibrils (CNF) were liberated from bleached softwood fibres from Domsjö dissolving, Domsjö Mill, Aditya Birla, Sweden, in the same manner as described by Fall *et al.*. A surface charge on the fibrils was introduced in a carboxymethylation process[30] prior to liberation. Furthermore, unfibrillated fibres and fibre fragments were removed during a centrifugation at 4750 rcf for 2h. The resulting transparent dispersion, having the concentration 1 g/L, was concentrated to the semi-dilute concentration of 3 g/L through evaporation at room conditions. MilliQ-water was used as the passive sheath solution with pH 7 while the pH was adjusted to 2 by adding HCl for the active second sheath solution.

2.2 Flow channel

The flow focusing device was built up of a sandwich structure having five layers, as is depicted in Fig. 1a. The first layer was an aluminum plate with a slit to make the channel visible and 20 threaded holes for screwing the device together. The second and fourth layers where 125 μm thick Kapton films in the SAXS experiments and 2 mm thick poly(methyl methacrylate) PMMA plates during the POM measurements. The third layer was a 1 mm thick stainless steel plate, in which the square channel with side $h = 1$ mm was cut out of. Lastly, the fifth layer was again an aluminum plate in order to keep the device rigid and non-leaking. Hoses were connected to the fifth layer and holes through the fourth layer connected the hoses to the channel in the stainless steal plate.

The channel in the steel plate seen in Fig. 1b, consisted of five inlets and one outlet, where the outlet was either connected to a hose (SAXS) or submerged in a water bath (POM) during the experiments. The inlets and the outlet were all more than 30 mm long in order to have fully developed flow in these regions. The distance between the two sheath channels was 4 mm.

Three syringe pumps (Aladdin 4000, WPI) was used to transfer the CNF-dispersion as well as the pH 7 and pH 2 solutions to the channel. The mass flow rates were: $Q_{core} = 1.1$ mm^3/s, $Q_{s1} = 2.6$ mm^3/s and $Q_{s2} = 13$ mm^3/s for all there experiments.

2.3 SAXS setup and orientation quantification

Small Angle X-ray Scattering (SAXS) was performed at the storage ring PETRA III at DESY in Hamburg, Germany. The P03 beamline[31,32] was used in a transmission setup with a sample to detector distance 8422 mm and X-ray wavelength $\lambda = 0.957$ Å. The beam size was 26×17 μm^2 (Horiz. $\times$ Vert.) and a single-photon counting detector (Pilatus 1M, Dectris) having the pixel size of 172×172 μm^2 was used to record the scattering diffractograms. One such scattering diffractogram is shown in Fig. 2a, where the intensity is shown in a logarithmic scale and the scattering vector, $q = 4\pi \sin(\zeta/2)/\lambda$, as well as the azimuthal angle ϕ are drawn. In order to find the orientation distribution, the diffractogram is transformed to show ϕ versus q, displayed in Fig. 2b, where the intensity is normalized at each q-value with the highest intensity. In Fig. 2c, the normalized intensity distributions are shown for $0.2 < q < 0.6$ (black lines in Fig. 2b), together with the mean (red line). This intensity distribution corresponds to the orientation distribution, $\Psi(\phi)$, of the fibrils at this location in the channel.

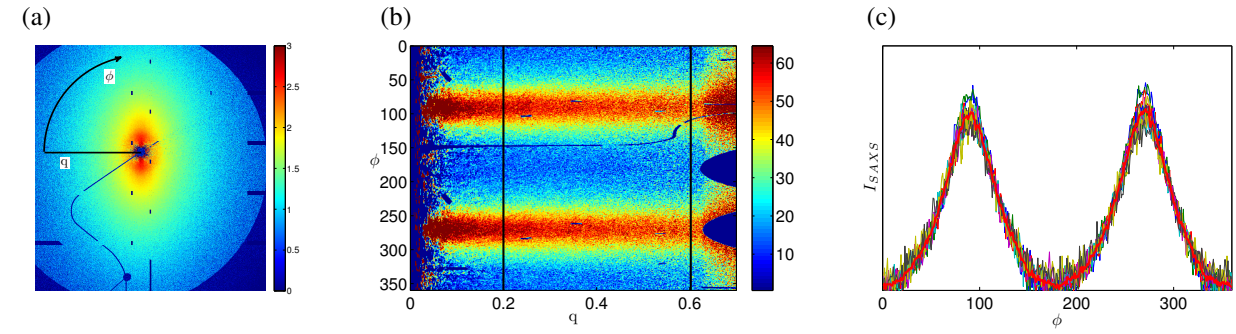

Fig. 2 A SAXS diffractogram is shown in (a) with a logarithmic color scale, where also q and ϕ are defined. In (b), the diffractorgram in (a) has been transformed to have q and ϕ as Cartesian coordinates. Each q column has also been normalized with its maximum value, and the color scale here is linear. The graph in (c) shows all normalized intensity distributions from (b) between $0.2 < q < 0.6$ (two black lines in (b)) The red line corresponds to the mean distribution.

In order to reduce the orientation distribution to a single number, the order parameter, S, defined by van Gurp as the mean of the second order Legendre polynomial, P_2, is used:

$$S = \langle P_2(\cos\phi)\rangle = \left\langle \frac{3}{2}\cos^2\phi - \frac{1}{2}\right\rangle. \quad (1)$$

This order parameter is a measure of the alignment of elongated particles, here in the z-direction, where $S = 1$ if all particles are aligned in the z-direction and $S = 0$ if the distribution is random. The measure can be related to the birefringence of the sample as described below, but when the distribution is known, S is calculated as:

$$S_{SAXS} = \int_0^\pi \Psi(\phi)\left(\frac{3}{2}\cos^2\phi - \frac{1}{2}\right)\sin\phi\ \mathrm{d}\phi, \quad (2)$$

and normalised according to:

$$\int_0^\pi \Psi(\phi)\sin\phi\ \mathrm{d}\phi = 1. \quad (3)$$

2.4 The Smoluchowski equation

Since SAXS experiments are expensive and time consuming, a model to describe the evolution of the orientation distribution of the fibrils, $\Psi(\mathbf{r},\mathbf{p},t)$, is wanted. After the extensional flows in the channel, only the Brownian rotary diffusion acts on the fibrils[4] and the orientation distribution can be modeled by the Smoluchowski equation (Eq. 4), which is a diffusive-convective equation. The orientation distribution is dependent on position, $\mathbf{r}$, orientation, $\mathbf{p}$, and time, t, and the equation reads:

$$\frac{D\Psi}{Dt} = \Re\hat{D}_r\cdot\Re\Psi. \quad (4)$$

Here, the rotary diffusion coefficient is denoted $\hat{D}_r(\mathbf{p},\mathbf{r})$ and $\Re$ is the rotational operator:

$$\Re = \mathbf{r}\times\frac{\partial}{\partial\mathbf{r}}. \quad (5)$$

As a simplified model, the flow was assumed to be axisymmetric, and the orientation distribution was only considered along the centreline in the z-direction, see the coordinate system shown in Fig. 1c. The Smolushowski equation can then be simplified to:

$$w^*\frac{\partial\Psi}{\partial z^*} = \frac{1}{\sin\phi}\frac{\partial}{\partial\phi}\left(\hat{D}_r^*\sin\phi\frac{\partial\Psi}{\partial\phi}\right), \quad (6)$$

in cylindrical coordinates, where w is the velocity in the z-direction, ϕ is defined in Fig. 1c. The star, *, denotes that the quantity has been non-dimensionalised with w and h. From the tube model proposed by Doi and Edwards, the rotary diffusion has been adapted to be dependent on the orientation as:

$$\hat{D}_r(\mathbf{p}) = D_r\left[\frac{4}{\pi}\int \mathrm{d}\mathbf{p}'|\mathbf{p}\times\mathbf{p}'|\Psi_s(\mathbf{p}')\right]^{-2}, \quad (7)$$

where D_r is a constant. Since both the velocity, w and the rotary diffusion, D_r, are unknown, one of the parameters can be set and the other one fitted to the experimental data. The velocity w was chosen to be 0.033 m/s, which would be the velocity at the centreline if the flow would be a fully developed laminar pipe flow, $2w_{mean} = 2(Q_{core}+Q_{s1}+Q_{s2})/h^2$, see Tritton. The other unknown parameter, D_r, is tuned to fit the experiments, and the three cases shown in Fig. 3 and Fig. 5 correspond to $D_r = 0.090, 0.119, 0.150$. Note that these exact numbers are not important and it is only the shape of the decaying orientation curve that will be used. The initial orientation distribution is taken from the SAXS experiments and the

equation is solved with periodic boundary conditions for the orientation distribution. The equation is solved numerically in MATLAB with the central differences method.

2.5 Birefringence and POM

The principle behind the polarized optical microscopy (POM) is to place a sample between two linear polarization filters. This setup makes it possible to quantify the birefringence of the sample. The light intensity, I, reaching a detector after the second filter can be expressed as:

$$I(\Delta\gamma) = I_0 \cos^2(\Delta\gamma + \gamma_0), \tag{8}$$

where, I_0 is the incoming intensity, $\Delta\gamma$ is the angle the polarization has been rotated by the sample and γ_0 is the angle between the two polarization filters[36]. Here, the filters are crossed and $\gamma_0 = 90°$. The angle the polarization is rotated, $\Delta\gamma$, is

$$\Delta\gamma = \frac{2\pi d}{\lambda}\Delta n, \tag{9}$$

where d is the distance that the light travels in the sample, λ is the wavelength of the incoming light, and Δn is the difference between the two refractive indices in the two different directions in the sample. Combining Eq. 8 and Eq. 9 gives:

$$\Delta n = \frac{\lambda}{2\pi d}\left(\cos^{-1}\sqrt{\frac{I}{I_0}} - \gamma_0\right) \approx \frac{\lambda}{2\pi d}\sqrt{\frac{I}{I_0}}, \tag{10}$$

for small I, and $\Delta\gamma << 90°$.

The order parameter, S, introduced above can also be determined with POM as[33]:

$$S_{POM} = \frac{\Delta n}{\Delta n_{max}}, \tag{11}$$

which means that the ratio between the order parameter, S, in two experiments is proportional to the square root of the intensity ratio of the two cases, provided the depth, d, is constant:

$$\frac{S}{S_{ref}} = \frac{\Delta n}{\Delta n_{ref}} \approx \sqrt{\frac{I}{I_{ref}}}. \tag{12}$$

The order parameter from POM and SAXS experiments has in previous studies been confirmed to correspond to the same quantity by for example Hongladarom *et al.*.

The polarization filters are placed at an angle of 45° in a plane parallel with the mean flow, see white arrows in Fig. 1b, in order to maximize the birefringence signal. The full POM set-up consisted of a light source (Schott, KL2500 LCD), two polarization filters, a stereo microscope (Nikon, SMZ 1500) and a camera (Basler, piA1900-32gm) controlled via Labview. The mean of 900 images was used and a background image was subtracted before the images were analyzed.

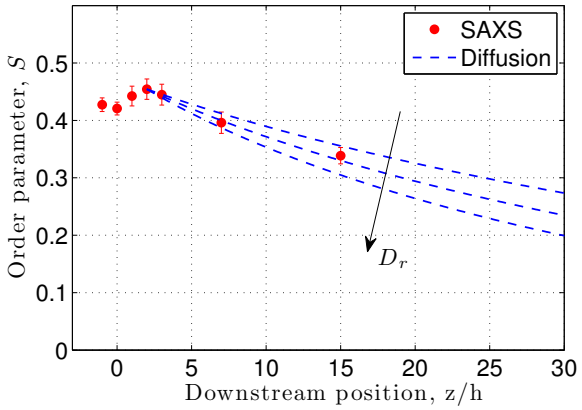

Fig. 3 Quantified SAXS data (red dots) and rotary diffusion calculations (blue dashed curves) of the order parameter, S, as function of downstream position along the centerline of the channel. The three different blue dashed lines represent $D_r = 0.090, 0.119, 0.150$.

2.6 Scanning Electron Microscopy, SEM

A dry filament was produced and firstly coated with a 10 nm thick gold-palladium layer by a commercial sputterer (Cressington Scientific Instruments Ltd, UK), whereafter, a Scanning Electron Microscope (S-4800 Field Emission-Scanning Electron Microscope, Hitachi, Japan) was used to image the filament surface in the secondary electron imaging mode at an acceleration voltage of 1kV.

3 Results and Discussion

Fibrils have been shown to align in the flow direction in the domain of extensional flow in a flow focusing device[4,22]. Thereafter, the fibrils de-align due to rotary Brownian diffusion. In this set-up the CNF is subjected to two extensional flows, the first in order for the CNF dispersion to detach from the walls in the channel and thereby, as explained below, avoid clogging of gel, and the second to increase the alignment. The second sheath fluid also carries ions, that are allowed to diffuse into the CNF dispersion and trigger a phase transition to gel. The detachment is illustrated in Fig. 1b, and is necessary for this process to run continuously. If the CNF is in contact with the wall when the phase transition occurs, a build up of the gel will start at this position and would soon clog the apparatus.

The SAXS measurements from experiment (i) are quantified with the order parameter, S. The results at different downstream positions are shown in Fig. 3 with red dots, where the

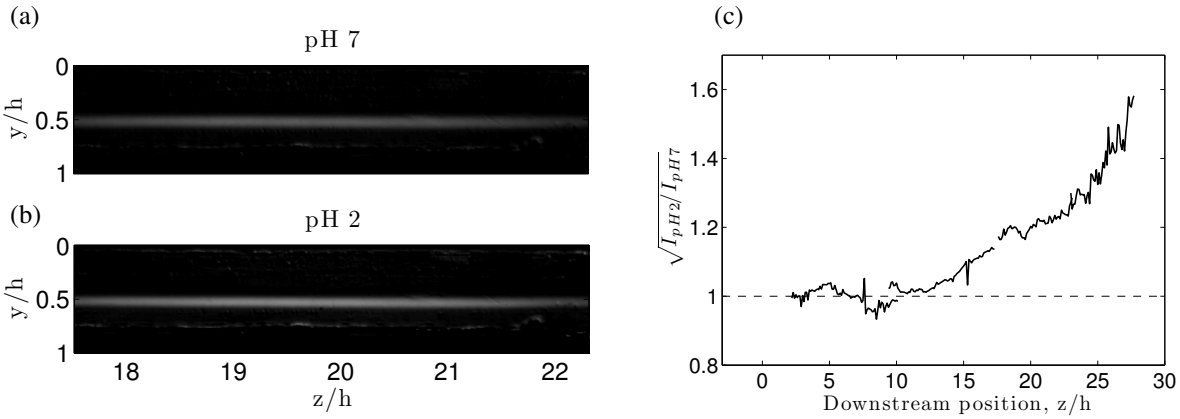

Fig. 4 Images of the flow in the channel between two crossed polarization filters are shown in (a) and (b). The second sheath flow is has a pH of 7 in (a) and pH 2 in (b). In (c) the square root of the intensity ratio between the second and third experiment are shown versus downstream position in the channel (solid line). This ratio is also the ratio of the order parameter between the two cases. The dashed line highlights the value 1.

error bars represent the standard deviation between different q-values. The alignment (order parameter) measurements confirm that the fibrils align due to the extensional flows ($z/h < 2$) and when no force from the flow is acting on the fibrils, they tend to de-align ($z/h > 2$), due to Brownian motion. In this experiment, both the first and second sheath flows consist of deionized water with pH 7 and no gelation occurs. Due to the first extension ($-4 < z/h < -2$), the alignment is already around $S = 0.41$ as the fibrils enter the second extensional flow at $z/h = 0$ where the alignment is modestly increased. The order parameter upstream of the first focusing ($z/h < -5$) must be lower than $S = 0.19$, as was the case in previous experiment[4], since the velocity here is lower and hence less shear is present in this study. The maximum alignment (order parameter) is reached at around $z/h = 2$, at the end of the extensional flow. After the extensional flow, Brownian rotary diffusion alone is forcing the fibrils back towards de-alignment. The Brownian diffusion is in this paper modeled by the Smoluchowski equation[34], see Eq. 4, with the initial distribution being that from the SAXS measurements at $z/h = 2$. The three blue dashed lines in Fig. 3 are calculations with different values of the rotary diffusion coefficient, D_r. The middle line gives a good estimation of the orientation distribution evolution along the center of the channel after the two extensional flows.

In order to determine at which orientation and downstream position the gelation occurs, two experiments with polarized light were conducted, (ii) and (iii). Experiment (ii) is the reference case with no gelation (same as in the SAXS experiments) and (iii) is the process case with the second sheath flow having pH 2 resulting in a gel thread. In Fig. 4a and Fig. 4b, images from the two cases are shown, pH 7 in a and pH 2 in b. At this downstream position one can clearly see that the intensity of light is higher in the case of pH 2 (iii), which is the result of a stronger alignment, remember that higher light intensity means higher alignment, see Eq. 10 and Eq. 11. Furthermore, Eq. 12 reveals that the order parameter ratio is proportional to the square root of the intensity ratio if the depth is constant. Since the flow is the same in both cases, this is a valid assumption regarding the depth. By scanning the channel (see Fig. 1b) it is possible to acquire intensities from both cases and in Fig. 4c, $\sqrt{I_{pH2}/I_{pH7}}$ is plotted. The ratio is expected to be around 1, until the protons, H^+, from the pH 2 solution in experiment (iii) has had time to diffuse into the core flow. The ratio, $\sqrt{I_{pH2}/I_{pH7}}$, is indeed around one for $z/h < 12$, whereafter the ratio is increasing. Thus, the location of the gelation can be determined to be around $z/h \approx 12$, where the curve detaches from 1. The increased noise in the signal, downstream in the channel, is due to the fact that when the order decreases the light intensity of the pH 7 case, (ii), approaches zero. Since this is only a relative measure, it is not possible to deduce the absolute orientation from this data alone. However, by combining these results with the SAXS-results, an absolute measure of the gel thread order is possible to determine.

In Fig. 5, the red dots are again the SAXS results and the blue dashed line is the diffusion calculation as before (Fig. 3). The black line is the POM ratio displayed in Fig. 4b with assumption that the pH 7 case behaves as the diffusion calculation (blue dashed horizontal line), which in turn was matched to the SAXS measurements in Fig. 3. At the position $z/h \approx 12$ the black line is seen to assume the constant value of ≈ 0.36 (brown dashed line), indicating that the rotary diffusion no longer is active and that the structure is *in fact* completely locked by the gelation.

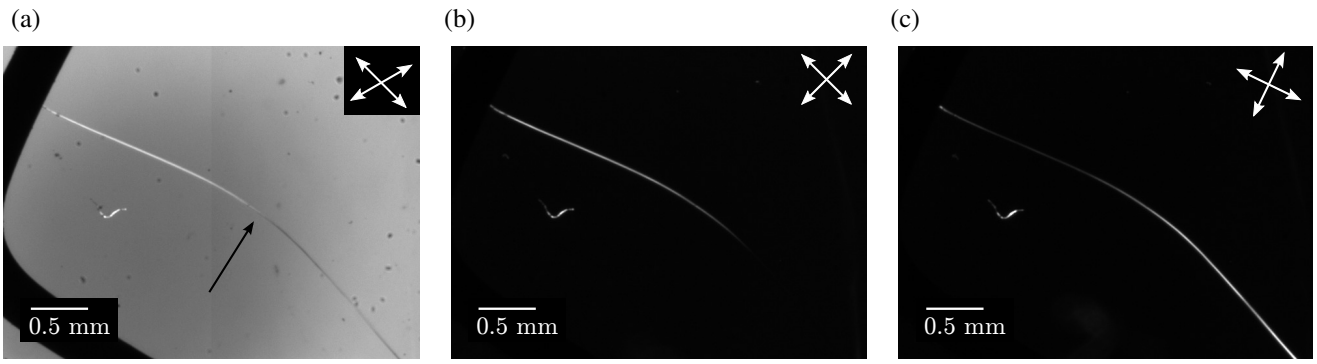

Fig. 6 The black arrow in (a) points at a hydrogel thread in water, which is placed between two polarization filters (orientation indicated by white arrows). The polarization filters are almost crossed in (a) and crossed in (b) and (c). The black dots in (a) are dirt on the lens and the bright spot seen in all three images is dust in the water bath.

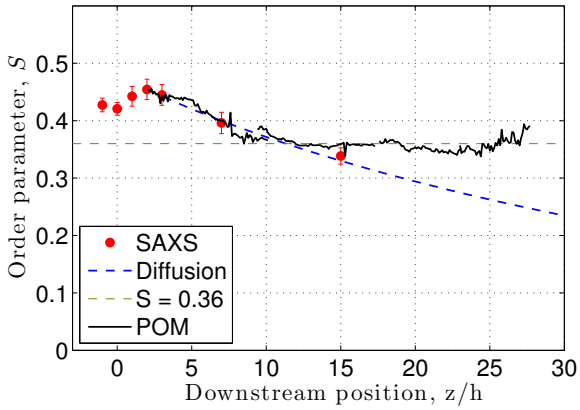

Fig. 5 Quantified SAXS data (red dots), diffusion calculations (blue dashed line) and POM data (black line). The diffusion calculations are assumed to be the true de-alignment of the reference case and the POM gelation measurement (black line) are then seen to assume a constant value (≈ 0.36, dashed brown line), downstream in the channel.

In the ideal structuring process, the extension should align all fibrils in the flow direction bringing the order parameter to 1, whereafter the fibrils would only be subjected to Brownian diffusion. If that was the case, by controlling the pH of the second sheath flow and also the flow rate it should be possible to control the gelation location and then also the order parameter, S, of the gel thread. By for example having a lower pH, the diffusion time of the necessary ions to reach the dispersion would decrease and the resulting gel thread would have a higher anisotropy. In the case presented here, even at an extension of 15 times ($(Q_{core}+Q_{s1}+Q_{s2})/Q_{core}=15.2$), the maximum order is not more than $S=0.45$, which indicates difficulties to make a hydrogel with a higher order (more anisotropic nano-structure). However, it should be possible to lock the order at any location in the channel and thus also any order below the maximum of $S=0.45$. In order to lock the orientation at the highest order, one could decrease the pH in the second sheath flow as discussed above, which would decrease the time until enough ions have been diffused into the thread and then move the location of the gelation upstream. It is then also important to note that the location of gelation should not occur before the extensional flow is completed, as this would not allow for the fibrils to align.

In addition to the experiment in the channel, a CNF hydrogel thread was produced in the flow focusing device and stored in a water bath for six months. The thread was then placed between two polarization filters and photographed, the images are displayed in Fig. 6. The black arrow in Fig. 6a points at the thread and the white arrows shows the orientation of the polarization filters. The full thread is seen in Fig. 6a, where the polarization filters are not completely crossed, however, when the filters are crossed, the background is black and it is only where a birefringent material is present that light is able to arrive to the CCD-sensor in the camera, as in Fig. 6b and 6c. In Fig. 6b the orientation of the first filter is matched with the orientation of the thread in the lower right corner. Since the fibrils are aligned in the direction of the thread, the optical axis of the thread is aligned with one of the polarization filters and the polarization of the light is unaffected by the thread, the thread is not visible. However, in the upper left corner of the image in Fig. 6b, the thread is not aligned with the filters, and the anisotropy of the thread gives rise to a rotation of the polarization, which is seen as light in the image. In Fig. 6c, the first polarization filter is aligned with the thread in the upper left corner, and now, the thread lights up in the lower right

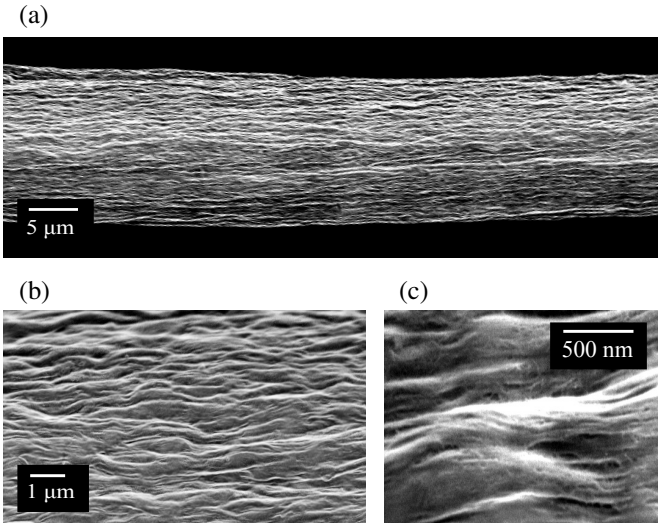

Fig. 7 Scanning electron microscopy images of a dried thread at three different magnifications are shown in (a)-(c). Ridges on the micrometer scale are clearly visible in all three images and individual fibrils can be seen in (c).

corner. This is an evidence of the birefringence, and shows that the optical axis is in the direction of the thread[36]. Even after the thread has been stored in a wet state for six months, it shows a birefringent behavior and, hence, the thread is still anisotropic.

The hydrogel thread was furthermore dried and Scanning Electron Microscopy (SEM) images of a dry thread (filament) at different magnification are displayed in Figs. 7a - 7c. The thread was not allowed to shrink in the direction of the thread during drying and a collapse of the hydrogel structure was observed in the radial direction, as the thickness significantly decreased. The dry thread is straight and the surface features, which include ridges and valleys, are similar to the features seen on other filaments recently produced from CNF[4,15,16]. A network of individual fibrils is visible at the highest magnification in Fig. 7c, however, the alignment of the fibrils is difficult to quantify by SEM images of the filament surface, and a succeeding study on the effect of drying, on the alignment of the fibrils, would be highly relevant for future filament production.

4 Conclusions

In conclusion, the filament manufacturing technique proposed by Håkansson *et al.*, was used to create hydrogels with detectable anisotropy (internal nano-structure of the fibrils). The combination of SAXS and POM measurements made it possible to determine the location and at which order parameter, *S*, the transition from dispersion to gel occurred. It was seen that the anisotropy was locked in the channel, and also that an alignment of the CNF was still present after storing the hydrogel for six months in a wet state. This characterization technique makes it possible to optimize the process[4] which aims at continuously producing a nano-structured bio-based filament as stiff and strong as nature creates wood fibres[8,9]. Furthermore, the technique to determine the anisotropy and anisotropy evolution described here should also be useful to other non-spherical particles exposed to similar flow focusing setups, such as polymers[38], DNA[22], silk proteins[5] and collagen[39] as long as a birefringence signal can be detected, in order to understand and later control the nano-structure during assembly.

Acknowledgements

A. B. Fall is acknowledged for the help with preparing the CNF. M. Kvick, A. B. Fall, L. Prahl Wittberg, F. Lundell and L. D. Söderberg are greatly acknowledged for the many discussions and execution of the SAXS experiments. L. Wågberg is acknowledged for all input during our discussions. F. Bark is greatly acknowledged for the discussions and input during the writing of the manuscript. Parts of this research were carried out at the light source PETRA III at DESY, a member of the Helmholtz Association (HGF). I would like to thank S. Yu and G. Santoro for assistance in using beamline P03. S. Yu is furthermore acknowledged for assistance with the scanning electron microscopy images. K. Karlström and G. Rådberg manufactured the flow cell and other experimental material. Innventia is greatly acknowledged for supplying the CNF. The Knut and Alice Wallenberg foundation through the Wallenberg Wood Science Center is acknowledged for the financial support.

References

1 S. J. Eichhorn, A. Dufresne, M. Aranguren, N. E. Marcovich, J. R. Capadona, S. J. Rowan, C. Weder, W. Thielemans, M. Roman, S. Renneckar, W. Gindl, S. Veigel, J. Keckes, H. Yano, K. Abe, M. Nogi, A. N. Nakagaito, A. Mangalam, J. Simonsen, A. S. Benight, A. Bismarck, L. A. Berglund and T. Peijs, *J. Mater. Sci.*, 2010, **45**, 1–33.

2 A. B. Fall, S. B. Lindström, J. Sprakel and L. Wågberg, *Soft Matter*, 2013, **9**, 1852.

3 M. M. Hamedi, A. Hajian, A. B. Fall, K. Håkansson, M. Salajkova, F. Lundell, L. Wågberg and L. A. Berglund, *ACS Nano*, 2014, **3**, 2467–2476.

4 K. M. O. Håkansson, A. B. Fall, F. Lundell, S. Yu, C. Krywka, S. V. Roth, G. Santoro, M. Kvick, L. Prahl Wittberg, L. Wågberg and L. D. Söderberg, *Nat. Commun.*, 2014, **5**, 4018.

5 M. E. Kinahan, E. Filippidi, S. Köster, X. Hu, H. M. Evans, T. Pfohl, D. L. Kaplan and J. Wong, *Biomacromolecules*, 2011, **12**, 1504–1511.

6 K. E. Shopsowitz, H. Qi, W. Y. Hamad and M. J. MacLachlan, *Nature*, 2010, **468**, 422–426.

7 R. T. Olsson, M. A. S. Azizi-Samir, G. Salazar-Alvarez, L. Belova, V. Ström, L. A. Berglund, O. Ikkala, J. Nogues and U. W. Gedde, *Nat. Nanotechnol.*, 2010, **5**, 584–588.

8 D. H. Page, F. el Hosseiny and K. Winkler, *Nature*, 1971, **229**, 252–253.

9 D. H. Page and F. el Hosseiny, *J. Pulp. Paper. Sci.*, 1983, 99–100.

10 I. Burgert, J. Keckes, K. Fruhmann, P. Fratzl and S. E. Tschegg, *Plant Biol.*, 2002, **4**, 9–12.

11 M. Eder, O. Arnould, J. W. C. Dunlop, J. Hornatowska and L. Salmén, *Wood Sci. Technol.*, 2013, **47**, 163–182.

12 T. Saito, R. Kuramae, J. Wohlert, L. A. Berglund and A. Isogai, *Biomacromolecules*, 2012, **14**, 248–253.

13 I. Sakurada, Y. Nubushina and T. Ito, *J. Polym. Sci.*, 1962, **57**, 651–660.

14 M. Henriksson, L. A. Berglund, P. Isaksson, T. Lindström and T. Nishino, *Biomacromolecules*, 2008, **9**, 1579–1585.

15 S. Iwamoto, A. Isogai and T. Iwata, *Biomacromolecules*, 2011, **12**, 831–836.

16 A. Walther, J. V. I. Timonen, I. Diez, A. Laukkanen and O. Ikkala, *Adv. Mater.*, 2011, **23**, 2924–2928.

17 H. Sehaqui, N. E. Mushi, S. Morimune, M. Salajkova, T. Nishino and L. A. Berglund, *Appl. Mater. Interfaces*, 2012, **4**, 1043–1049.

18 M. Pääkkö, M. Ankerfors, H. Kosonen, A. Nykänen, S. Ahola, M. Österberg, J. Ruokolainen, J. Laine, P. T. Larsson, O. Ikkala and T. Lindström, *Biomacromolecules*, 2007, **8**, 1934–1941.

19 A. B. Fall, S. B. Lindström, O. Sundman, L. Ödberg and L. Wågberg, *Langmuir*, 2011, **27**, 11332–11338.

20 J. B. Knight, A. Vishwanath, J. P. Brody and R. H. Austin, *Phys. Rev. Lett.*, 1998, **80**, 3863–3866.

21 S. Anna, N. Bontoux and H. A. Stone, *Appl. Phys. Lett.*, 2003, **82**, 364–366.

22 T. Pfohl, A. Otten, S. Köster, R. Dootz, B. Struth and H. M. Evans, *Biomacromolecules*, 2007, **8**, 2167–2172.

23 P. J. A. Kenis, R. F. Ismagilov and G. M. Whitesides, *Science*, 1999, **285**, 83–84.

24 G. B. Jeffery, *Proc. R. Soc. London A*, 1922, **102**, 161–179.

25 E. S. G. Shaqfeh and D. L. Koch, *Phys. Fluids*, 1990, **2**, 1077–1093.

26 A. L. Thangawng, P. B. Howell Jr., J. J. Richards, J. S. Erickson and F. S. Ligler, *Lab Chip*, 2009, **9**, 3126–3130.

27 J. Puigmarti-Luis, D. Schaffhauser, B. R. Burg and P. S. Dittrich, *Adv. Mater.*, 2010, **22**, 2255–2259.

28 D. A. Boyd, A. R. Shields, P. B. Howell Jr. and F. S. Ligler, *Lab Chip*, 2013, **13**, 3105–3110.

29 M. E. Brennich, J.-F. Nolting, C. Dammann, B. Nöding, S. Bauch, H. Herrmann, T. Pfohl and S. Köster, *Lab Chip*, 2011, **11**, 708–716.

30 L. Wågberg, L. Winter, L. Ödberg and T. Lindström, *Colloids Surf.*, 1987, **27**, 163–173.

31 A. Buffet, A. Rothkirch, R. Döhrmann, V. Körstgens, M. M. A. Kashem, J. Perlich, G. Herzog, M. Schwartzkopf, R. Gehrke, P. Müller-Buschbaum and S. V. Roth, *J. Synchr. Radiation*, 2012, **19**, 647–653.

32 C. Krywka, H. Neubauer, M. Priebe, T. Salditt, J. Keckes, A. Buffet, S. V. Roth, R. Doehrmann and M. Mueller, *J. Appl. Crystallogr.*, 2012, **45**, 85.

33 M. van Gurp, *Colloid Polym. Sci.*, 1995, **273**, 607–625.

34 M. Doi and S. Edwards, *The theory of polymer dynamics*, Oxford University Press Inc., 1986.

35 D. J. Tritton, *Physical Fluid Dynamics*, Oxford Science Publications, 2nd edn, 2005.

36 E. Hecht, *Optics*, Addison Wesley, 4th edn, 2002.

37 K. Hongladarom, V. M. Ugaz, D. K. Cinader, W. R. Burghardt, J. P. Quintana, B. S. Hsiao, M. D. Dadmun, W. A. Hamilton and P. D. Butler, *Macromolecules*, 1996, **29**, 5346–5355.

38 A. R. Shields, C. M. Spillmann, J. Naciri, P. B. Howell Jr., A. L. Thangawng and F. S. Ligler, *Soft Matter*, 2012, **8**, 6656.

39 S. Köster, H. M. Evans, J. Y. Wong and T. Pfohl, *Biomacromolecules*, 2008, **9**, 199–207.